

Nearly model independent constraints on dense matter equation of state in a Bayesian approach

N. K. Patra^{1,*} , Sk Md Adil Imam^{2,3†} , B. K. Agrawal^{2,3**} , Arunava Mukherjee^{2,3+*}  and Tuhin Malik^{4,‡} 

¹ Department of Physics, BITS-Pilani, K. K. Birla Goa Campus, Goa 403726, India.

² Saha Institute of Nuclear Physics, 1/AF Bidhannagar, Kolkata 700064, India.

³ Homi Bhabha National Institute, Anushakti Nagar, Mumbai 400094, India.

⁴ CFisUC, Department of Physics, University of Coimbra, 3004-516 Coimbra, Portugal.

* Correspondence: bijay.agrawal@saha.ac.in;

Abstract: We apply Bayesian approach to construct a large number of minimally constrained equations of state (EoSs) and study their correlations with a few selected properties of neutron star (NS). Our set of minimal constraints includes a few basic properties of saturated nuclear matter and low density pure neutron matter EoS which is obtained from a precise next-to-next-to-next-to-leading order (N^3LO) calculation in chiral effective field theory. The tidal deformability and radius of NS with mass $1-2M_\odot$ are found to be strongly correlated with the pressure of β -equilibrated matter as well as with the symmetry energy at densities higher than the saturation density ($\rho_0 = 0.16 \text{ fm}^{-3}$) in a nearly model independent manner. These correlations are employed to parametrize the pressure for β -equilibrated matter, around $2\rho_0$, as a function of neutron star mass and the corresponding tidal deformability. The maximum mass of neutron star is also strongly correlated with the pressure of symmetric and β -equilibrated matter at densities $\sim 4.5\rho_0$.

Keywords: Neutron Star; Equation of State; β -Equilibrium Matter; Symmetric Nuclear Matter; Bayesian Parameter Estimation

1. Introduction

Gravitational-wave astronomy promises unprecedented constraints on the EoS of neutron star matter through the detailed properties of gravitational waveform observed during the merging of binary neutron stars (BNS). The tidal deformability parameters inferred from these gravitational wave events encodes information about the EoS. For the first time, BNS event (GW170817) was observed by LIGO-Virgo detector from a low mass compact binary neutron star merger with a total mass of the system $2.74_{-0.01}^{+0.04} M_\odot$ [1,2]. Another gravitational wave event likely originating from the coalescence of BNS, GW190425, is observed [3] subsequently. These two events have already triggered many theoretical investigations to constrain the EoS of neutron star matter [3–12]. The upcoming runs of LIGO-Virgo-KAGRA and the future detectors, e.g., Einstein Telescope (ET) and Cosmic Explorer (CE), are expected to observe many more BNS signals emitted from coalescing neutron stars. The mass and radius of NS, observed either in isolation or in binaries, by the Neutron star Interior Composition Explorer (NICER) [13–15] have offered complementary constraints on the EoS. A sufficiently large number of such observations over a wide range of NS mass may be employed to constrain several key quantities associated with the EoS of β -equilibrated matter which are not readily accessible in the terrestrial laboratory. The behaviour of the EoS at supra-saturation densities are generally studied using the observed maximum neutron star mass, together with radius and tidal deformability corresponding to the neutron star with canonical mass $1.4M_\odot$ [16–18]. Recently in Ref. [19–24], efforts are made to constrain the EoS of β -equilibrated matter which is relevant to the studies of NS properties. The values of tidal deformability of NS with mass $1-2M_\odot$ are found to be strongly correlated with the EoS at twice the saturation density.

Statistical tools are quite helpful in providing a quantitative interpretation of NS observables. A Bayesian approach is often applied to analyze gravitational-wave signals, which involves nearly fifteen



Citation: Patra, N. K.; Imam, Sk Md Imam.; Agrawal, B. K.; Mukherjee, Arunava.; Malik, Tuhin. Nearly model independent constraints on dense matter equation of state in a Bayesian approach. *Preprints* **2021**, *1*, 0. <https://doi.org/>

Received:

Accepted:

Published:

Publisher's Note: MDPI stays neutral with regard to jurisdictional claims in published maps and institutional affiliations.

parameters for binary compact object mergers, to infer their source properties [25]. It has been also extended to investigate the properties of short gamma-ray burst [26], neutron star [27–29], the formation history of binary compact objects [30–34] and to test general relativity [35–38]. Of late, Bayesian approach has become a useful statistical tool for parameter estimation in the field of nuclear physics and nuclear-astronomy [39]. It allows one to obtain joint posterior distributions of the model parameters and the correlations among them for a given set of data. Various constraints on the parameters known *a priori* are incorporated through their prior distributions. The Bayesian techniques have also been employed to constrain symmetry energy [40], masses and radii of NS [41] using the bounds on the EoS obtained from chiral effective field theory. The Bayesian techniques have been extensively applied to constrain the EoS for symmetric nuclear matter (SNM), β -equilibrated matter (BEM) and density dependence of symmetry energy coefficient using various finite nuclei and NS properties [42–53].

We use Bayesian approach to construct large sets of EoSs which correspond to the Taylor and $\frac{n}{3}$ expansions [53]. The expansion coefficients in the former case are the individual nuclear matter parameters (NMPs), whereas in the latter case it is their linear combinations. The EoSs are consistent with a set of minimal constraints that includes a few low order nuclear matter parameters at the saturation density and EoS for the pure neutron matter (PNM) at low densities obtained from a precise next-to-next-to-next-to-leading order (N^3LO) calculation in chiral effective field theory. The marginalized posterior distributions of NMPs and the various NS properties obtained from set of minimal constraints are found to be within reasonable bounds. The correlations of various NS properties, such as tidal deformability, radius and maximum mass, with key EoS parameters are studied. These correlations are investigated for a wide range of NS mass and density for the EoS.

The paper is organized as follows, the Taylor and $\frac{n}{3}$ expansions for the EoS of neutron star matter and the Bayesian approach are briefly outlined in Sec. 2. The results for the posterior distributions of NMPs and associated NS properties together with their correlations with some key quantities associated with EoS are presented in Sec. 3. The main outcomes of the present investigation are summarized in the Sec. 4.

2. Methodology

The energy per nucleon for neutron star matter $E(\rho, \delta)$ at a given total nucleon density ρ and asymmetry δ can be decomposed into the energy per nucleon for the SNM, $E(\rho, 0)$ and the density-dependent symmetry energy, $E_{\text{sym}}(\rho)$ in the parabolic approximation as,

$$E(\rho, \delta) = E(\rho, 0) + E_{\text{sym}}(\rho)\delta^2 + \dots, \quad (1)$$

where, $\delta = \left(\frac{\rho_n - \rho_p}{\rho}\right)$ with ρ_n and ρ_p being the neutron and proton densities, respectively. The value of δ at a given ρ is determined by the condition of β -equilibrium and the charge neutrality. Once δ is known, the fraction of neutron, proton, electron, muon can be easily evaluated. In the following, we expand $E(\rho, 0)$ and $E_{\text{sym}}(\rho)$ appearing in Eq. (1) using Taylor and $\frac{n}{3}$ expansions. The coefficients of expansion in case of the Taylor correspond to the individual nuclear matter parameters. In the latter case, they are expressed as linear combinations of the nuclear matter parameters.

2.1. Taylor's expansion

The $E(\rho, 0)$ and $E_{\text{sym}}(\rho)$ can be expanded around the saturation density ρ_0 as [54–58],

$$E(\rho, 0) = \sum_n \frac{a_n}{n!} \left(\frac{\rho - \rho_0}{3\rho_0}\right)^n, \quad (2)$$

$$E_{\text{sym}}(\rho) = \sum_n \frac{b_n}{n!} \left(\frac{\rho - \rho_0}{3\rho_0}\right)^n, \quad (3)$$

so that,

$$E(\rho, \delta) = \sum_n \frac{1}{n!} (a_n + b_n \delta^2) \left(\frac{\rho - \rho_0}{3\rho_0} \right)^n, \quad (4)$$

where the coefficients a_n and b_n are the nuclear matter parameters. We truncate the sum in Eqs. (2) and (3) at 4th order, i.e., $n = 0 - 4$. Therefore, the coefficients a_n and b_n correspond to,

$$a_n \equiv \varepsilon_0, 0, K_0, Q_0, Z_0, \quad (5)$$

$$b_n \equiv J_0, L_0, K_{\text{sym},0}, Q_{\text{sym},0}, Z_{\text{sym},0}. \quad (6)$$

In Eqs. (5) and (6), ε_0 is the binding energy per nucleon, K_0 the incompressibility coefficient, J_0 the symmetry energy coefficient, its slope parameter L_0 , $K_{\text{sym},0}$ the symmetry energy curvature parameter, Q_0 ($Q_{\text{sym},0}$) and Z_0 ($Z_{\text{sym},0}$) are related to third and fourth order density derivatives of $E(\rho, 0)$ ($E_{\text{sym}}(\rho)$), respectively. The subscript zero indicates that all the NMPs are calculated at the saturation density.

It may be noticed from Eq. (4) that the coefficients a_n and b_n may display some correlations among themselves provided the asymmetry parameter depends weakly on the density. Further, the Eq. (4) may converge slowly at high densities, i.e., $\rho \gg 4\rho_0$. This situation is encountered for the heavier neutron stars. The neutron stars with a mass around $2M_\odot$, typically have central densities $\sim 4 - 6\rho_0$.

2.2. $\frac{n}{3}$ expansion

Alternative expansion of $E(\rho, \delta)$ can be obtained by expanding $E(\rho, 0)$ and $E_{\text{sym}}(\rho)$ as [59,60],

$$E(\rho, 0) = \sum_{n=2}^6 (a'_{n-2}) \left(\frac{\rho}{\rho_0} \right)^{\frac{n}{3}}, \quad (7)$$

$$E_{\text{sym}}(\rho) = \sum_{n=2}^6 (b'_{n-2}) \left(\frac{\rho}{\rho_0} \right)^{\frac{n}{3}}, \quad (8)$$

$$E(\rho, \delta) = \sum_{n=2}^6 (a'_{n-2} + b'_{n-2} \delta^2) \left(\frac{\rho}{\rho_0} \right)^{\frac{n}{3}}. \quad (9)$$

We refer this as the $\frac{n}{3}$ expansion. It is now evident from Eqs.(7) and (8) that the coefficients of expansion are no-longer the individual nuclear matter parameters unlike in case of Taylor's expansion. The values of the NMPs can be expressed in terms of the expansion coefficients a' and b' as,

$$\begin{pmatrix} \varepsilon_0 \\ 0 \\ K_0 \\ Q_0 \\ Z_0 \end{pmatrix} = \begin{pmatrix} 1 & 1 & 1 & 1 & 1 \\ 2 & 3 & 4 & 5 & 6 \\ -2 & 0 & 4 & 10 & 18 \\ 8 & 0 & -8 & -10 & 0 \\ -56 & 0 & 40 & 40 & 0 \end{pmatrix} \begin{pmatrix} a'_0 \\ a'_1 \\ a'_2 \\ a'_3 \\ a'_4 \end{pmatrix}, \quad (10)$$

$$\begin{pmatrix} J_0 \\ L_0 \\ K_{\text{sym},0} \\ Q_{\text{sym},0} \\ Z_{\text{sym},0} \end{pmatrix} = \begin{pmatrix} 1 & 1 & 1 & 1 & 1 \\ 2 & 3 & 4 & 5 & 6 \\ -2 & 0 & 4 & 10 & 18 \\ 8 & 0 & -8 & -10 & 0 \\ -56 & 0 & 40 & 40 & 0 \end{pmatrix} \begin{pmatrix} b'_0 \\ b'_1 \\ b'_2 \\ b'_3 \\ b'_4 \end{pmatrix}. \quad (11)$$

The relations between the expansion coefficients and the NMPs are governed by the nature of functional form for $E(\rho, 0)$ and $E_{sym}(\rho)$. The off-diagonal elements in the above matrices would vanish for the Taylor's expansion of $E(\rho, 0)$ and $E_{sym}(\rho)$ as given by Eqs. (2) and (3), respectively. Therefore, each of the expansion coefficients are simply the individual NMPs given by Eqs. (5) and (6). Inverting the matrices in Eqs. (10) and (11) we have,

$$\begin{aligned}
a'_0 &= \frac{1}{24}(360\varepsilon_0 + 20K_0 + Z_0), \\
a'_1 &= \frac{1}{24}(-960\varepsilon_0 - 56K_0 - 4Q_0 - 4Z_0), \\
a'_2 &= \frac{1}{24}(1080\varepsilon_0 + 60K_0 + 12Q_0 + 6Z_0), \\
a'_3 &= \frac{1}{24}(-576\varepsilon_0 - 32K_0 - 12Q_0 - 4Z_0), \\
a'_4 &= \frac{1}{24}(120\varepsilon_0 + 8K_0 + 4Q_0 + Z_0), \\
b'_0 &= \frac{1}{24}(360J_0 - 120L_0 + 20K_{sym,0} + Z_{sym,0}), \\
b'_1 &= \frac{1}{24}(-960J_0 + 328L_0 - 56K_{sym,0} - 4Q_{sym,0} \\
&\quad - 4Z_{sym,0}), \\
b'_2 &= \frac{1}{24}(1080J_0 - 360L_0 + 60K_{sym,0} + 12Q_{sym,0} \\
&\quad + 6Z_{sym,0}), \\
b'_3 &= \frac{1}{24}(-576J_0 + 192L_0 - 32K_{sym,0} - 12Q_{sym,0} \\
&\quad - 4Z_{sym,0}), \\
b'_4 &= \frac{1}{24}(120J_0 - 40L_0 + 8K_{sym,0} + 4Q_{sym,0} \\
&\quad + Z_{sym,0}).
\end{aligned} \tag{12}$$

Each of the coefficients a' and b' are the linear combinations of nuclear matter parameters in such a way that the lower-order parameters may contribute dominantly at low densities. The effects of higher-order parameters become prominent with the increase in density.

2.3. Bayesian estimation of nuclear matter parameters

A Bayesian approach enables one to carry out detailed statistical analysis of the parameters of a model for a given set of fit data. It yields joint posterior distributions of model parameters which can be used to study not only the distributions of given parameters but also to examine correlations among model parameters. One can also incorporate prior knowledge of the model parameters and various constraints on them through the prior distributions. This approach is mainly based on the Bayes theorem which states that [61],

$$P(\theta|D) = \frac{\mathcal{L}(D|\theta)P(\theta)}{\mathcal{Z}}, \tag{14}$$

where θ and D denote the set of model parameters and the fit data. The $P(\theta|D)$ is the joint posterior distribution of the parameters, $\mathcal{L}(D|\theta)$ is the likelihood function, $P(\theta)$ is the prior for the model parameters and \mathcal{Z} is the evidence. The posterior distribution of a given parameter can be obtained by marginalizing $P(\theta|D)$ over remaining parameters. The marginalized posterior distribution for a parameter θ_i can be obtained as,

$$P(\theta_i|D) = \int P(\theta|D) \prod_{k \neq i} d\theta_k. \quad (15)$$

We use Gaussian likelihood function defined as,

$$\mathcal{L}(D|\theta) = \prod_j \frac{1}{\sqrt{2\pi\sigma_j^2}} e^{-\frac{1}{2} \left(\frac{d_j - m_j(\theta)}{\sigma_j} \right)^2}. \quad (16)$$

Here the index j runs over all the data, d_j and m_j are the data and corresponding model values, respectively. The σ_j are the adopted uncertainties. The evidence \mathcal{Z} in Eq. (14) is obtained by complete marginalization of the likelihood function. It is relevant when employed to compare different models. However in the present work \mathcal{Z} is not very relevant. To populate the posterior distribution of Eq. (14), we implement a nested sampling algorithm by invoking the Pymultinest nested sampling [62] in the Bayesian Inference Library [25].

3. Results and Discussions

We obtained the EoSs for symmetric nuclear matter (SNM) and β -equilibrated matter (BEM) using Taylor and $\frac{n}{3}$ expansions as discussed in previous section. The coefficients of the Taylor expansion are the individual nuclear matter parameters, whereas, they correspond to linear combinations of nuclear matter parameters for the $\frac{n}{3}$ expansion. We construct marginalised PDs for the NMPs by applying a Bayesian approach to both the expansions considered. The NMPs or the corresponding EoSs are consistent with a set of minimal constraints that includes basic properties of saturated nuclear matter and low density EoS for the PNM from (N³LO) calculation in chiral effective field theory. These large number of EoSs are employed to evaluate the NS properties such as tidal deformability, radius and maximum mass. The correlations of neutron star properties with the pressure of BEM and SNM as well as with the symmetry energy coefficient at a given density are studied. Most of these correlation are sensitive to the choice of the NS mass and the density of EoS. Our results for the correlations of tidal deformability with pressure for BEM are analogous to those obtained using a diverse set of non-relativistic and relativistic mean-field models emphasizing their model independence. These model independent trends enable us to parametrize the pressure for BEM around $2\rho_0$ in terms of NS mass and the corresponding tidal deformability.

3.1. Posterior distribution of nuclear matter parameters

To undertake the correlation systematics as proposed, we need a large number of EoSs with diverse behaviour and corresponding NS properties. We apply Bayesian approach to obtain two large sets of EoSs corresponding to the Taylor and $\frac{n}{3}$ expansions. These EoSs at a given density and asymmetry essentially depends on the NMPs. The posterior distributions for the NMPs are obtained by subjecting the EoS to a set of minimal constraints which include some basic properties of nuclear matter evaluated at the saturation density ρ_0 and EoS for the PNM at low density. The NMPs which are constrained within narrow bounds are the binding energy per nucleon $\varepsilon_0 = -16.0 \pm 0.3$ MeV, nuclear matter incompressibility coefficients $K_0 = 240 \pm 50$ MeV for the SNM and symmetry energy coefficient $J_0 = 32.0 \pm 5$ MeV. These NMP's are derived from the bulk properties of finite nuclei [63,64]. The low density EoS for the PNM employed is obtained from a precise next-to-next-to-next-to-leading order (N³LO) calculation in chiral effective field theory [65]. The joint posterior distribution of the NMPs for a given model depends on the product of the likelihood and the prior distribution of NMPs Eq.(14). The constraints on the NMPs are incorporated through the prior distribution as listed in Table 1. The prior distributions of ε_0, K_0, J_0 are assumed to be Gaussian with rather smaller width, whereas, the other NMPs correspond to Gaussian distribution with very large width. The information about the EoS for the PNM are incorporated through a simple likelihood function as given by Eq.(16). The posterior distribution of each individual parameter can be obtained by marginalizing the joint

posterior distribution with the remaining model parameters. If the marginalized posterior distribution of a parameter is localized more than the corresponding prior distribution, then, the parameter is said to be well constrained by the data used for model fitting. The data we use for the PNM of our EoS at the very low density range is taken from chiral effective field theory [65]. We further filter the NMP's by demanding that (i) symmetry energy should increase monotonically with density (ii) pressure for the SNM should also increase monotonically with density above saturation density ρ_0 .

Table 1: The prior distributions of the nuclear matter parameters (in MeV). The nuclear matter considered are the binding energy per nucleon (ϵ_0), incompressibility coefficient (K_0), symmetry energy coefficient (J_0), it's slope parameter (L_0), symmetry energy curvature parameter ($K_{\text{sym},0}$) and $Q_0(Q_{\text{sym},0})$ and $Z_0(Z_{\text{sym},0})$ are related to third and fourth order density derivatives of $E(\rho, 0)$ ($J(\rho)$), respectively. All the nuclear matter parameters are evaluated at saturation density $\rho_0 = 0.16 \text{ fm}^{-3}$. The parameters of Gaussian distribution (G) are the mean (μ) and standard deviation (σ).

| Parameters | Pr-Dist | μ | σ |
|--------------------|---------|-------|----------|
| ϵ_0 | G | -16 | 0.3 |
| K_0 | G | 240 | 50 |
| Q_0 | G | -400 | 400 |
| Z_0 | G | 1500 | 1500 |
| J_0 | G | 32 | 5 |
| L_0 | G | 50 | 50 |
| $K_{\text{sym},0}$ | G | -100 | 200 |
| $Q_{\text{sym},0}$ | G | -550 | 400 |
| $Z_{\text{sym},0}$ | G | -2000 | 2000 |

The corner plots for the marginalized PDs for the NMPs in one and two dimensions obtained for Taylor and $\frac{n}{3}$ expansions for the EoSs are displayed in Fig.1. The difference between the one-dimensional PDs for the NMPs and corresponding prior distributions reflect the role of low density EoS for pure neutron matter in constraining the NMPs. The shapes and the orientations of the confidence ellipses suggest that the correlations among most of NMPs are weak. Most Strong correlations exist only between $Q_0 - Z_0$, $L_0 - J_0$ and $L_0 - K_{\text{sym},0}$ for both the models with correlation coefficient $r \simeq 0.8$. However, $K_0 - Q_0$ correlation is found to be stronger in case of $\frac{n}{3}$ expansion. The median values of the NMPs and the corresponding 68%(90%) confidence intervals obtained from the marginalized PDs are listed in Table 2. We also provide the values for the NMPs obtained without the PNM constraints. The low density PNM mainly constraints those NMPs which are associated with the density-dependence of the symmetry energy. The median values of L_0 and $K_{\text{sym},0}$, which determined the linear and quadratic density-dependence of the symmetry energy, become smaller suggesting softer symmetry energy with the inclusion of PNM constraints. Further, the uncertainties on L_0 reduced by more than 50%. The median values of $Q_{\text{sym},0}$ and $Z_{\text{sym},0}$ remain more or less unaltered. The L_0 has been determined to be $106 \pm 37 \text{ MeV}$ [66] from the recent measurement of the neutron skin thickness of ^{208}Pb nucleus [66,67], $\Delta R_{\text{skin}} = 0.283 \pm 0.071 \text{ fm}$, through PREX-II measurements. This value of L_0 agrees with the ones obtained in the present work with PNM constrain only within 90% confidence interval.

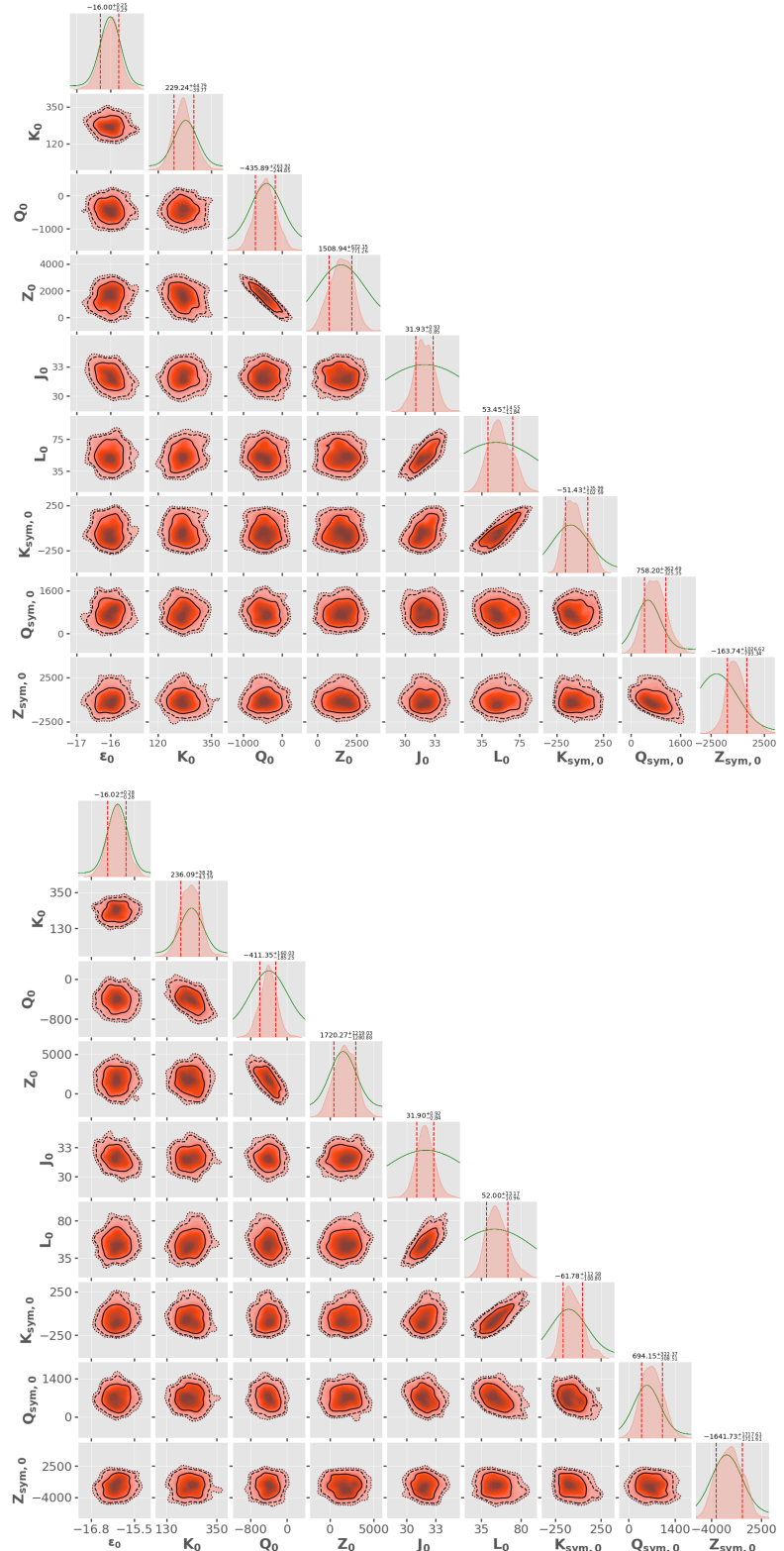


Figure 1. Corner plots for the nuclear matter parameters obtained for Taylor (top) and $\frac{n}{3}$ (bottom) expansions for the EoS of asymmetric nuclear matter. The one dimensional marginalized posterior distributions (salmon) and the prior distributions (green lines) are displayed along the diagonal plots. The vertical lines indicate 68% confidence interval of nuclear matter parameters. The confidence ellipses for two-dimensional posterior distributions are plotted with 1σ , 2σ and 3σ confidence intervals along the off diagonal plots. The distributions of nuclear matter parameters are obtained by subjecting them to minimal constraints (see text for details).

Table 2: The median values and associated 68%(90%) uncertainties for the nuclear matter parameters (in MeV) from their marginalized posterior distributions. The results are obtained for Taylor and $\frac{n}{3}$ expansions with and without pure neutron matter (PNM) constraints.

| NMPs | Without PNM | | With PNM | |
|--------------------|--------------------------------------------------|----------------------------------------------------|--------------------------------------------------|----------------------------------------------------|
| | Taylor | $\frac{n}{3}$ | Taylor | $\frac{n}{3}$ |
| ϵ_0 | $-16.01^{+0.23(0.40)}_{-0.24(0.46)}$ | $-16.02^{+0.27(0.41)}_{-0.23(0.53)}$ | $-16.00^{+0.25(0.45)}_{-0.29(0.57)}$ | $-16.02^{+0.28(0.48)}_{-0.28(0.57)}$ |
| K_0 | $238.51^{+43.56(65.11)}_{-47.08(81.32)}$ | $229.08^{+42.57(67.60)}_{-38.83(77.25)}$ | $229.24^{+44.79(78.39)}_{-39.77(76.39)}$ | $236.09^{+38.29(62.04)}_{-43.39(82.09)}$ |
| Q_0 | $-443.98^{+280.76(455.67)}_{-274.45(524.36)}$ | $-398.58^{+181.33(298.56)}_{-178.62(380.93)}$ | $-435.89^{+263.92(436.68)}_{-244.85(491.48)}$ | $-411.35^{+160.03(278.39)}_{-185.25(354.78)}$ |
| Z_0 | $1449.01^{+723.65(1224.64)}_{-685.39(1368.10)}$ | $1696.07^{+1160.80(1933.13)}_{-1258.78(2219.10)}$ | $1508.44^{+672.15(1075.85)}_{-771.62(1351.20)}$ | $1720.27^{+1219.03(1854.75)}_{-1280.88(2235.03)}$ |
| J_0 | $32.10^{+4.20(6.99)}_{-4.56(8.90)}$ | $32.03^{+4.51(7.32)}_{-4.21(9.13)}$ | $31.93^{+0.93(1.50)}_{-0.85(-1.82)}$ | $31.90^{+0.92(1.57)}_{-0.84(1.68)}$ |
| L_0 | $67.22^{+35.64(60.90)}_{-33.94(54.17)}$ | $57.56^{+37.52(69.89)}_{-31.88(52.92)}$ | $53.45^{+14.55(21.20)}_{-11.84(21.64)}$ | $52.00^{+13.77(23.10)}_{-10.96(20.45)}$ |
| $K_{\text{sym},0}$ | $-35.06^{+134.67(233.68)}_{-128.87(275.20)}$ | $-34.82^{+131.60(219.91)}_{-114.98(218.67)}$ | $-51.43^{+135.99(206.39)}_{-102.59(176.02)}$ | $-61.78^{+112.58(198.99)}_{-100.80(160.08)}$ |
| $Q_{\text{sym},0}$ | $723.35^{+319.54(512.01)}_{-326.72(681.47)}$ | $717.26^{+275.43(496.39)}_{-331.72(669.16)}$ | $758.20^{+362.49(624.95)}_{-325.35(609.30)}$ | $694.15^{+322.37(534.33)}_{-308.51(563.33)}$ |
| $Z_{\text{sym},0}$ | $-196.87^{+1105.87(2009.63)}_{-882.92(1634.09)}$ | $-1613.31^{+1453.59(2660.53)}_{-1734.18(3376.64)}$ | $-163.74^{+1026.62(2054.49)}_{-793.39(1709.54)}$ | $-1641.73^{+1717.61(2551.70)}_{-1711.61(3076.76)}$ |

3.2. Properties of neutron stars

Once the EoS for the core and crust are known the values of NS mass, radius and tidal deformability corresponding to given central pressure can be obtained by solving Tolman-Oppenheimer-Volkoff equations [68,69]. The EoSs for core region of neutron star, correspond to the β -equilibrated matter over the density range $0.5-8\rho_0$, are obtained from the posterior distributions of NMPs for the Taylor and $\frac{n}{3}$ expansions. The core EoSs are matched to the crust EoSs for obtaining the NS properties. The EoS for outer crust is taken to be the one given by Baym-Pethick-Sutherland [70]. The inner crust that joins the inner edge of the outer crust and the outer edge of the core is assumed to be polytropic [71], $p(\epsilon) = c_1 + c_2\epsilon^\gamma$. Here, the parameters c_1 and c_2 are determined in such a way that the EoS for the inner crust matches with the outer crust at one end ($\rho = 10^{-4} \text{ fm}^{-3}$) and with the core at the other end ($0.5\rho_0$). The polytropic index γ is taken to be equal to $4/3$. The radii of neutron star with mass $\sim 1M_\odot$ are more sensitive to the treatment of crust EoS [72]. It is demonstrated that the treatment of crust EoS employed in the present work may introduce the uncertainties of about 50-100 m in radii of NS having mass $1.4M_\odot$. It is shown in Ref. [73] that the choice of EoS for inner-crust does not significantly impact the values of tidal deformability which depends on the Love number k_2 as well as the compactness parameter.

We have obtained the distributions of $\Lambda_{1.4}, R_{1.4}, R_{2.07}$ and M_{max} using the marginalized PDs for the NMPs corresponding to the Taylor and $\frac{n}{3}$ expansions. The corner plots for these NS properties are displayed in Fig. 2. It is clear from off-diagonal plots that $\Lambda_{1.4}$ is strongly co-related with $R_{1.4}$, the correlation coefficients $r \sim 0.9$. The $\Lambda_{1.4}$ and $R_{1.4}$ also display stronger correlations with $R_{2.07}$ ($r \sim 0.8$) for the case of Taylor and some what moderate correlations ($r \sim 0.7$) for the $\frac{n}{3}$ expansion. The maximum mass of neutron star is almost uncorrelated with the other NS properties considered. The median values of NS properties along with 68% (90%) confidence intervals are listed in Table 3. Like in the case of NMPs, the NS properties get significantly constrained by the EoS of PNM at low density. For instance, the median values of $\Lambda_{1.4}$ become smaller by about 15% and the associate uncertainties by about 40% with the PNM constraints. The median values of $R_{1.4}$ and the corresponding uncertainties also become noticeably smaller. The $R_{2.07}$ and M_{max} do not show any significant changes with the inclusion of low density PNM constraints. With the PNM constraints, the median values with 90% confidence

interval overlap with the currently available bounds on the various NS properties, $\Lambda_{1.4} \in [70, 580]$ [4], $R_{1.4} \in [11.41, 13.61]$ km [74], $R_{2.07} \in [11.8, 13.1]$ km [75] and $M_{\max} \geq 2.09M_{\odot}$ [76].

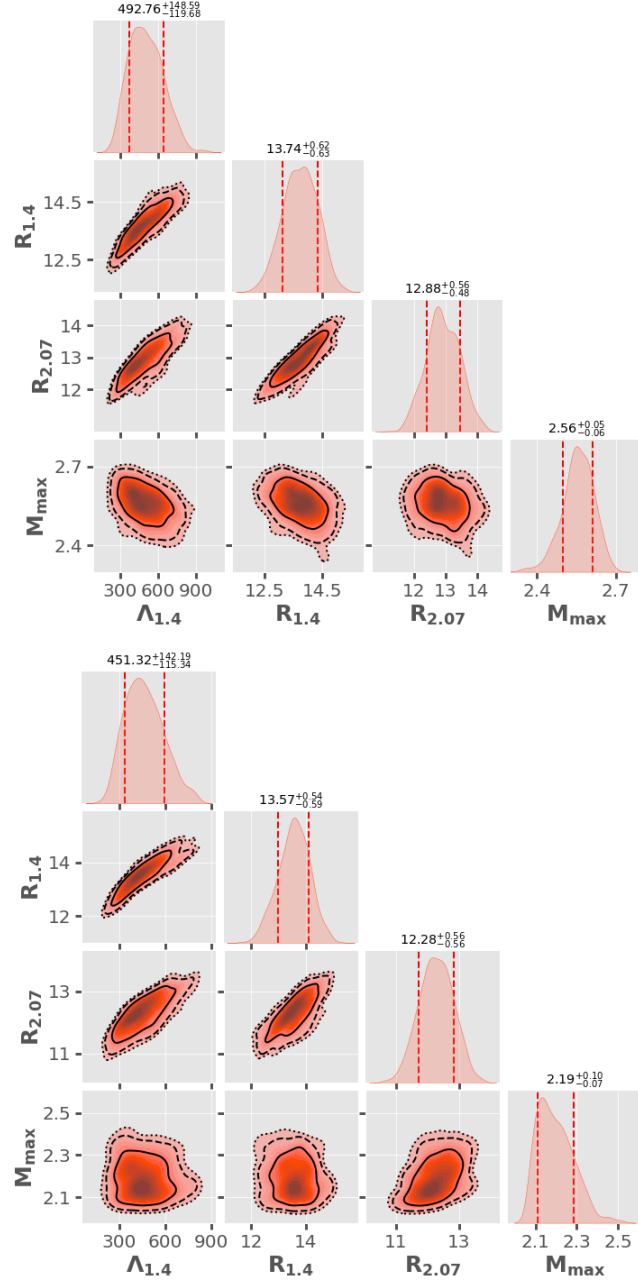


Figure 2. Same for Fig. 1, but, for the marginalized posterior distributions of neutron star properties, namely the tidal deformability $\Lambda_{1.4}$, radii $R_{1.4}$ and $R_{2.07}$ and the maximum mass M_{\max} for Taylor (top) and $\frac{n}{3}$ (bottom) expansions.

We obtain joint probability distribution $P(M, R)$ for a given mass and radius for both the Taylor and $\frac{n}{3}$ expansions. They display qualitatively very much similar trends. In Fig. 3, we plot the $P(M, R)$ obtained for the $\frac{n}{3}$ expansion. The 90% confidence interval is represented by red dashed line. The color gradient from orange to dark-purple represents the lowest to highest probability. The most probable values for $R_{1.4}$ and $R_{2.07}$ are approximately 13.5 and 12.2 km, respectively. The $P(M, R)$ is maximum

Table 3: Similar to Table 2, but, for the neutron star properties, namely the tidal deformability ($\Lambda_{1.4}$), radii ($R_{1.4}$ and $R_{2.07}$) (in km) and maximum mass (M_{\max}) (in M_{\odot}).

| Quantities | Without PNM | | with PNM | |
|-----------------|----------------------------------------------|----------------------------------------------|----------------------------------------------|----------------------------------------------|
| | Taylor | $\frac{n}{3}$ | Taylor | $\frac{n}{3}$ |
| $\Lambda_{1.4}$ | $554.00^{+229.99(503.80)}_{-155.55(275.75)}$ | $483.25^{+214.52(500.72)}_{-133.57(203.60)}$ | $492.76^{+148.59(242.84)}_{-119.68(201.88)}$ | $451.32^{+142.19(224.14)}_{-115.34(182.80)}$ |
| $R_{1.4}$ | $14.68^{+1.98(4.43)}_{-1.43(2.37)}$ | $14.14^{+2.07(4.24)}_{-1.20(2.10)}$ | $13.74^{+0.62(0.93)}_{-0.63(1.19)}$ | $13.57^{+0.54(0.91)}_{-0.59(1.21)}$ |
| $R_{2.07}$ | $13.24^{+0.89(1.68)}_{-0.76(1.28)}$ | $12.39^{+0.88(1.71)}_{-0.58(1.09)}$ | $12.88^{+0.56(0.85)}_{-0.48(0.97)}$ | $12.28^{+0.56(0.88)}_{-0.56(1.03)}$ |
| M_{\max} | $2.55^{+0.05(0.08)}_{-0.06(0.13)}$ | $2.17^{+0.10(0.19)}_{-0.07(0.09)}$ | $2.56^{+0.05(0.08)}_{-0.06(0.14)}$ | $2.18^{+0.10(0.16)}_{-0.07(0.10)}$ |

for $M \sim 1.8M_{\odot}$, $R \sim 12.8$ km. The 90% confidence interval has partial overlap with LIGO-Virgo estimations. The NICER data show significant overlap. It may be however pointed out that the main objective of the present work is to construct large sets of EoSs with diverse behaviour to assess various correlation systematics as follows.

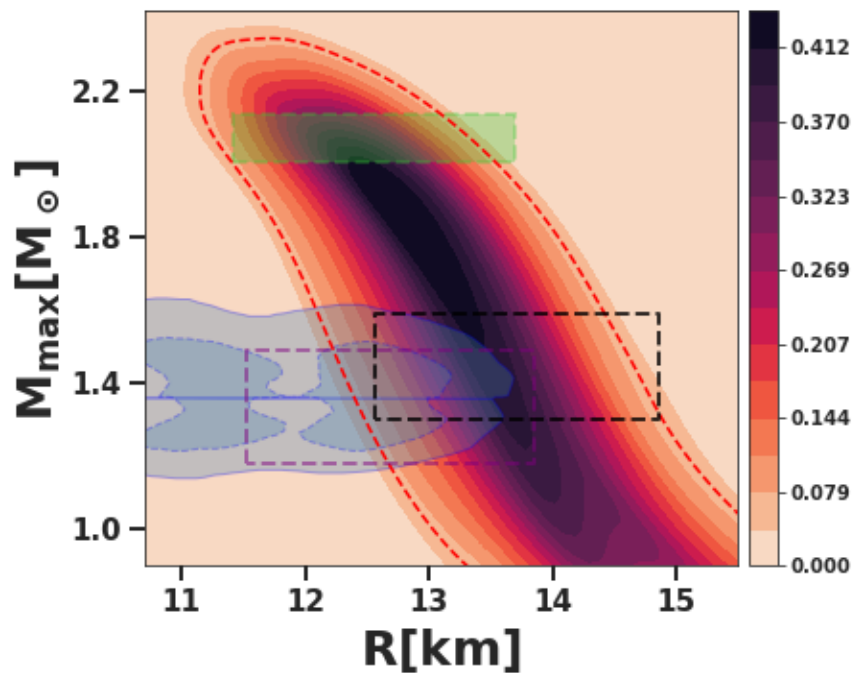


Figure 3. Plot for joint probability distribution $P(M, R)$ as a function of mass and radius of neutron star obtained for $\frac{n}{3}$ expansion. The red dashed line represents the 90% confidence interval. The outer and inner gray shaded regions indicate the 90% (solid) and 50% (dashed) confidence interval of the LIGO-Virgo analysis for BNS component from the GW170817 event [77–79]. The rectangular regions enclosed by dotted lines indicate the constraints from the millisecond pulsar PSR J0030+0451 (black & purple) NICER x-ray data [80,81] and PSR J0740+6620 (green) [75]

3.3. Correlations of neutron star properties with EoS

We randomly select 500 EoSs and corresponding NS properties from marginalized PDs obtained for the Taylor as well as $\frac{n}{3}$ expansions. They are used to study the correlations of various NS properties with key quantities determining the behaviour of the EoS. The correlations of $\Lambda_{1.4}$, $R_{1.4}$, $R_{2.07}$ and

M_{\max} with the pressure of β -equilibrated matter and symmetric nuclear matter as well as with the symmetry energy over a wide range of density are evaluated. The values of correlation coefficients are plotted as a function of density in Fig.4. We also display (top row) the values of correlation coefficients for NS properties with the pressure of β -equilibrated matter calculated using unified EoSs for a diverse set of 41 non-relativistic and relativistic microscopic mean field models [72]. The various NS properties considered show strong correlations with $P_{\text{BEM}}(\rho)$ around a particular density. The density at which the correlation is maximum increases with the NS mass. The pressure for SNM show strong correlation only with M_{\max} . The $E_{\text{sym}}(\rho)$ is strongly co-related with various NS properties at low mass and tends to disappear as the mass increases. This may be due to the fact that the matter is highly asymmetric at low densities and the asymmetry decreases with the increasing densities. The values of $\Lambda_{1.4}$ and $R_{1.4}$ are strongly correlated with P_{BEM} and E_{sym} at density $\sim 1.5\text{-}2.5\rho_0$. The $R_{2.07}$ is strongly correlated with P_{BEM} around $3\rho_0$. For the case of Taylor expansion, $R_{2.07}$ is also strongly correlated with P_{SNM} at $\rho \sim 3\rho_0$. The M_{\max} is strongly correlated with P_{BEM} and P_{SNM} around $4.5\rho_0$. Our results as plotted in the top row for the Taylor and $\frac{n}{3}$ expansions are in line with those obtained using a diverse set of mean field models which suggest the nature of correlations seem to be almost model independent.

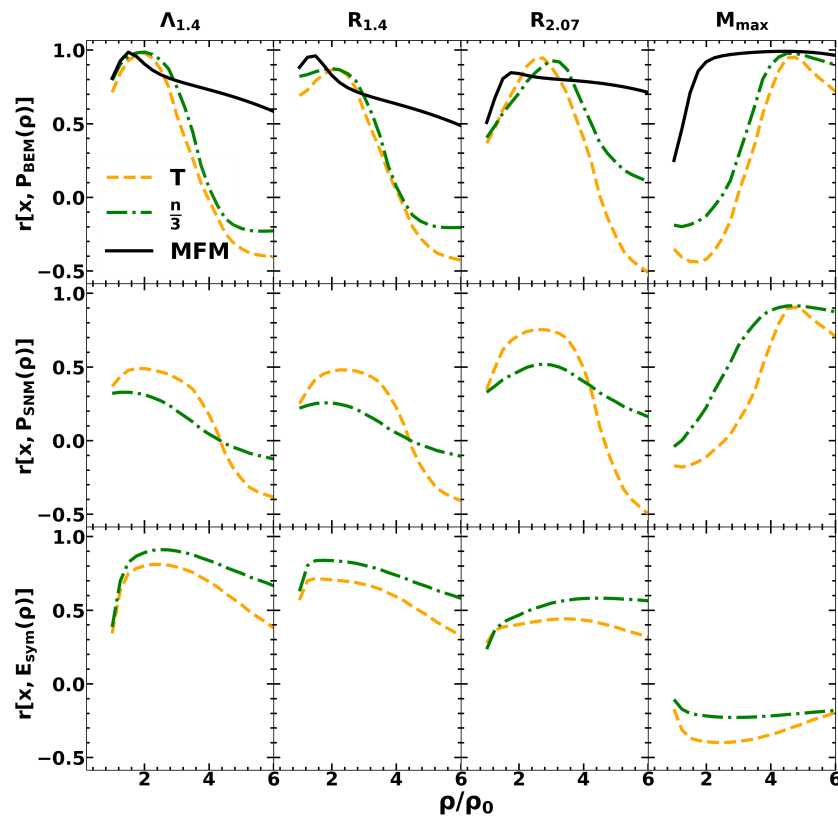


Figure 4. The correlation coefficients $r[x,y(\rho)]$ between x and $y(\rho)$, where x represents the tidal deformability $\Lambda_{1.4}$, radii $R_{1.4}$ and $R_{2.07}$, and maximum mass M_{\max} of neutron star, whereas, $y(\rho)$ represents the pressure for β -equilibrated matter (top), symmetric nuclear matter (middle) and symmetry energy (bottom) as a function of density. The calculations are performed with neutron star properties obtained using marginalized posterior distributions of nuclear matter parameters in Taylor and $\frac{n}{3}$ expansions. For the comparison the results are also displayed for a diverse set of non-relativistic and relativistic microscopic mean-field models (MFM) in the top panel.

In Table 4, we list the values of correlation coefficients obtained between the NS properties and the EoS at some selected densities. The correlation coefficients are obtained using 100 and 500 EoSs, corresponding to Taylor and $\frac{n}{3}$ expansions, randomly selected from the posterior distributions. We also present the results in the last column which are obtained by combining 500 EoSs corresponding to each of the expansions. The values of correlation coefficients for the combined set of EoSs are close to those obtained separately, except for M_{\max} . The correlation coefficients for the case of M_{\max} become larger when the results of Taylor and $\frac{n}{3}$ expansions are combined, because, the combine result spans wider range for the M_{\max} (see also Table 3). We plot in Fig. 5, the variations of P_{BEM} , P_{SNM} and E_{sym} at selected densities, with $\Lambda_{1.4}$, $R_{1.4}$, $R_{2.07}$ and M_{\max} for which the correlations are stronger.

Table 4: The comparison of values for Pearson's correlation coefficient (r) obtained from randomly selected 100 and 500 EoSs using both Taylor and $\frac{n}{3}$ expansions. The values of correlation coefficients are also obtained by combining 500 EoSs from each of the expansions.

| Name of Pairs | Taylor | | $\frac{n}{3}$ | | combined |
|-------------------------------------------|--------|------|---------------|------|----------|
| | 100 | 500 | 100 | 500 | 1000 |
| $\Lambda_{1.4}-P_{\text{BEM}}(2\rho_0)$ | 0.98 | 0.97 | 0.98 | 0.98 | 0.98 |
| $\Lambda_{1.4}-E_{\text{sym}}(2.5\rho_0)$ | 0.80 | 0.80 | 0.89 | 0.94 | 0.88 |
| $R_{1.4}-P_{\text{BEM}}(2\rho_0)$ | 0.89 | 0.86 | 0.85 | 0.90 | 0.88 |
| $R_{2.07}-P_{\text{BEM}}(3\rho_0)$ | 0.85 | 0.85 | 0.91 | 0.91 | 0.88 |
| $M_{\max}-P_{\text{BEM}}(4.5\rho_0)$ | 0.94 | 0.94 | 0.98 | 0.97 | 0.98 |
| $M_{\max}-P_{\text{SNM}}(4.5\rho_0)$ | 0.85 | 0.88 | 0.92 | 0.91 | 0.97 |

For the case of correlations of NS properties with the pressure of β -equilibrated matter, we compared our results with those obtained from a diverse set of mean field models. The correlation lines obtained by combining results of the Taylor and $\frac{n}{3}$ expansions are also plotted to estimate the values of P_{BEM} , P_{SNM} and E_{sym} at selected densities with help of NS properties. The equations for the correlation lines are obtained using linear regression as,

$$\frac{P_{\text{BEM}}(2\rho_0)}{\text{MeVfm}^{-3}} = (3.85 \pm 0.116) + (0.039 \pm 0.0002)\Lambda_{1.4}, \quad (17)$$

$$\frac{P_{\text{BEM}}(2\rho_0)}{\text{MeVfm}^{-3}} = (-81.56 \pm 1.89) + (7.67 \pm 0.13)\frac{R_{1.4}}{\text{km}}, \quad (18)$$

$$\frac{P_{\text{BEM}}(3\rho_0)}{\text{MeVfm}^{-3}} = (-207.58 \pm 4.21) + (23.83 \pm 0.33)\frac{R_{2.07}}{\text{km}}, \quad (19)$$

$$\frac{P_{\text{BEM}}(4.5\rho_0)}{\text{MeVfm}^{-3}} = (-973.03 \pm 9.71) + (561.86 \pm 4.07)\frac{M_{\max}}{M_{\odot}}, \quad (20)$$

$$\frac{P_{\text{SNM}}(4.5\rho_0)}{\text{MeVfm}^{-3}} = (-993.23 \pm 10.70) + (543.09 \pm 4.51)\frac{M_{\max}}{M_{\odot}}, \quad (21)$$

$$\frac{E_{\text{sym}}(2.5\rho_0)}{\text{MeV}} = (7.97 \pm 1.14) + (0.116 \pm 0.002)\Lambda_{1.4}. \quad (22)$$

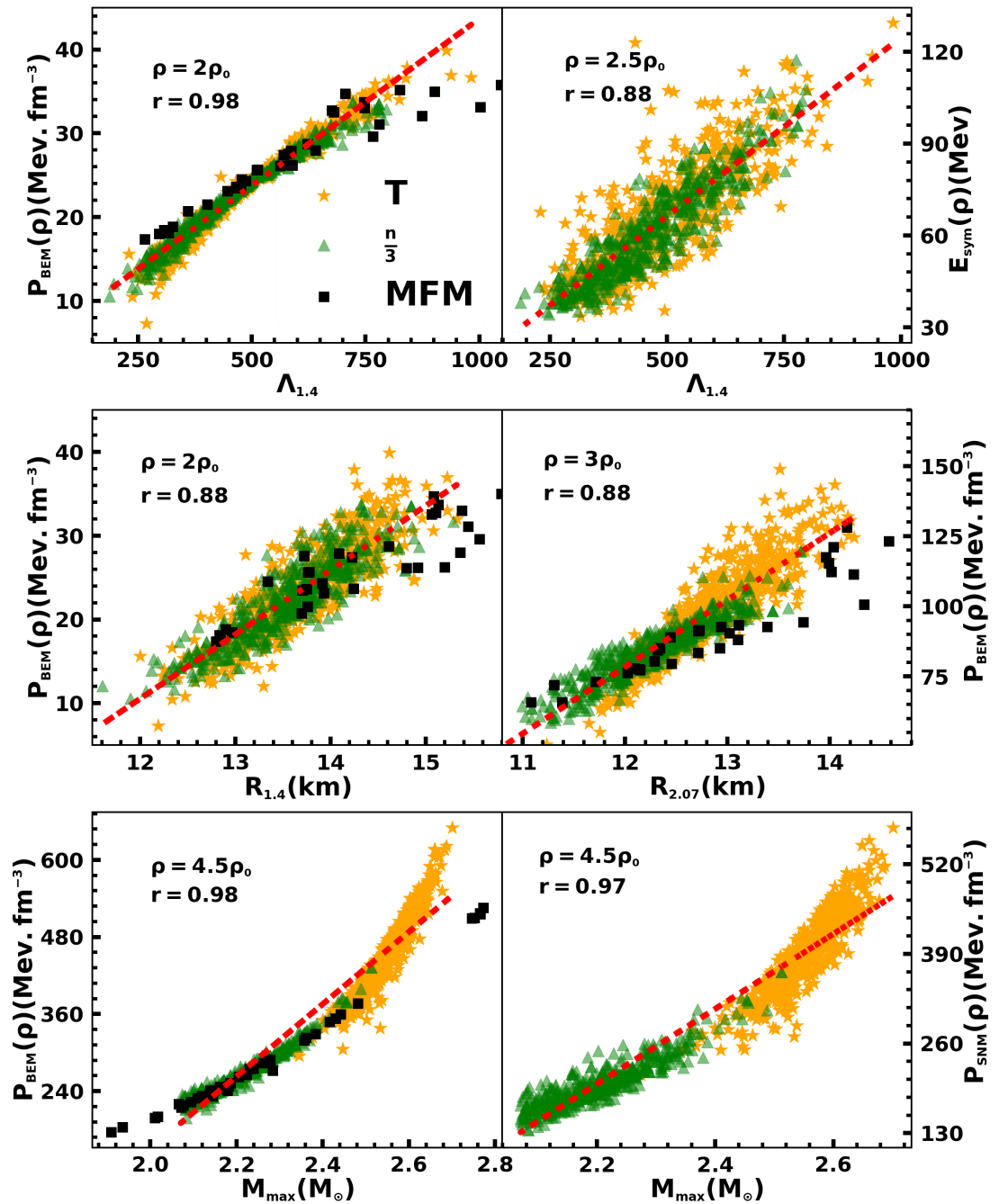


Figure 5. The variations of pressure for β -equilibrated matter, symmetric nuclear matter and symmetry energy at selected densities versus tidal deformability $\Lambda_{1.4}$, radii $R_{1.4}$ and $R_{2.07}$ and maximum mass M_{\max} of neutron star. The red dashed lines are obtained by linear regression.

We extend our analysis for the correlations of the pressure for the β -equilibrated matter with tidal deformability over a wide range of neutron star mass. In Fig. 6, we display color coded graph for the correlations of tidal deformability of neutron star for the mass 1.2-2.0 M_\odot with the pressure for β -equilibrated matter at densities 0.5-5 ρ_0 . One can easily obtain the value of correlation coefficient

as a function of density at a given NS mass. The $P_{\text{BEM}}(\rho)$ at $\rho \sim 1.5 - 2.5\rho_0$ are strongly correlated ($r \sim 0.8 - 1$) with tidal deformability for NS mass in the range $1.2-2 M_\odot$.

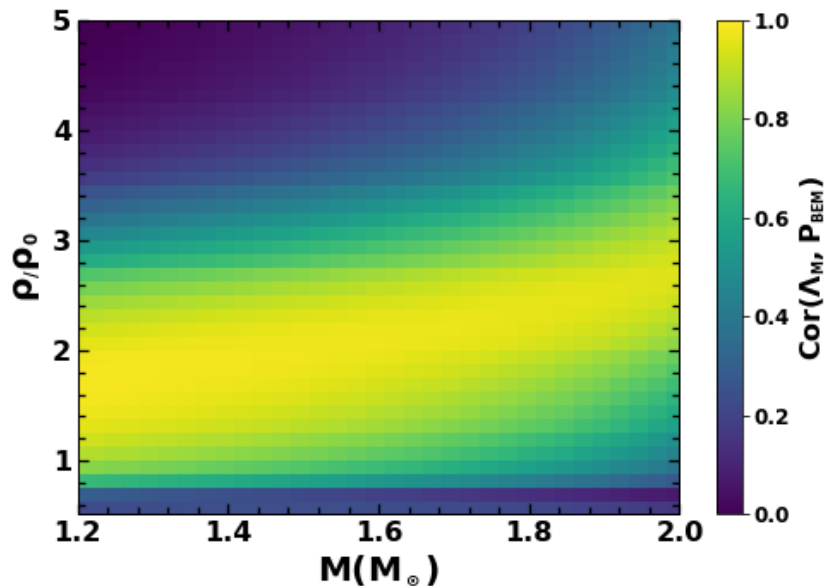


Figure 6. Colour coded plot for neutron star mass and density depicting the dependence of correlation coefficients between tidal deformability and the pressure of β -equilibrated matter.

These correlations suggest that $P_{\text{BEM}}(\rho)$ can be parametrized at a given ρ as,

$$P_{\text{BEM}}(\rho) = \left(a_0 + a_1(M - M_0) + a_2(M - M_0)^2 \right) + \left(b_0 + b_1(M - M_0) + b_2(M - M_0)^2 \right) \Lambda_M. \quad (23)$$

Where, M_0 is taken to be $1.4M_\odot$ and the values of a_i and b_i are estimated using a Bayesian approach with the help of $P_{\text{BEM}}(\rho)$ and tidal deformability obtained for Taylor and $\frac{n}{3}$ expansions. For a given ρ , the Eq.(23) is fitted using the tidal deformability corresponding to NS mass $1.2-2M_\odot$. The prior for a_i and b_i are taken to be uniform in the range of -100 to 100 . The calculations are performed for $\rho = 1.5, 2.0$ and $2.5\rho_0$. The median values of parameters a_i and b_i and associated uncertainties are summarized in Table 5. To validate our parametrized form for $P_{\text{BEM}}(\rho)$, we have calculated the values of $P_{\text{BEM}}(2\rho_0)$ using Eq.(23) with the help of tidal deformability for $1.4M_\odot$ obtained for large number of mean field models which includes the once considered in Fig. 5 along with those taken from [23,82,83]. The average deviation of $P_{\text{BEM}}(2\rho_0)$, obtained using Eq.(23), from the actual values is about 10%. We find marginal improvement when the terms corresponding to quadratic in tidal deformability are included in Eq.(23).

Table 5: The median values and associated 68%(90%) uncertainties for the parameters (in MeV fm⁻³), appearing in Eq. (23), obtained from their marginalized posterior distributions. The values of parameters b_0 , b_1 and b_2 as listed are scaled up by a factor of 10.

| Quantities | a_0 | a_1 | a_2 | b_0 | b_1 | b_2 |
|-----------------------------|------------------------------------------|-------------------------------------------|------------------------------------------|-----------------------------------------|-----------------------------------------|-----------------------------------------|
| $P_{\text{BEM}}(1.5\rho_0)$ | $0.874^{+0.053(0.087)}_{-0.053(0.106)}$ | $2.295^{+0.320(0.529)}_{-0.302(0.618)}$ | $11.728^{+0.701(1.167)}_{-0.675(1.374)}$ | $0.181^{+0.001(0.001)}_{-0.001(0.002)}$ | $0.746^{+0.007(0.011)}_{-0.007(0.014)}$ | $1.073^{+0.022(0.036)}_{-0.022(0.043)}$ |
| $P_{\text{BEM}}(2\rho_0)$ | $2.945^{+0.053(0.089)}_{-0.052(0.101)}$ | $0.080^{+0.309(0.522)}_{-0.306(0.616)}$ | $34.191^{+0.699(1.179)}_{-0.681(1.354)}$ | $0.416^{+0.001(0.001)}_{-0.001(0.002)}$ | $1.832^{+0.006(0.011)}_{-0.007(0.014)}$ | $2.789^{+0.022(0.036)}_{-0.022(0.044)}$ |
| $P_{\text{BEM}}(2.5\rho_0)$ | $16.567^{+0.053(0.088)}_{-0.052(0.106)}$ | $-12.582^{+0.315(0.526)}_{-0.321(0.627)}$ | $73.919^{+0.696(1.156)}_{-0.701(1.370)}$ | $0.686^{+0.001(0.001)}_{-0.001(0.002)}$ | $3.316^{+0.007(0.011)}_{-0.007(0.014)}$ | $5.402^{+0.022(0.037)}_{-0.022(0.043)}$ |

In Fig. 7, we display the variations of tidal deformability as a function of mass and pressure for β -equilibrated matter at $\rho=1.5, 2.0$ and $2.5\rho_0$. These results are obtained using the parametrized form for $P_{\text{BEM}}(\rho)$ as given by Eq. (23). One can easily estimate the values of $P_{\text{BEM}}(\rho)$ for $\rho \sim 2\rho_0$ once the values of tidal deformability known in NS mass ranges $1.2-2M_\odot$.

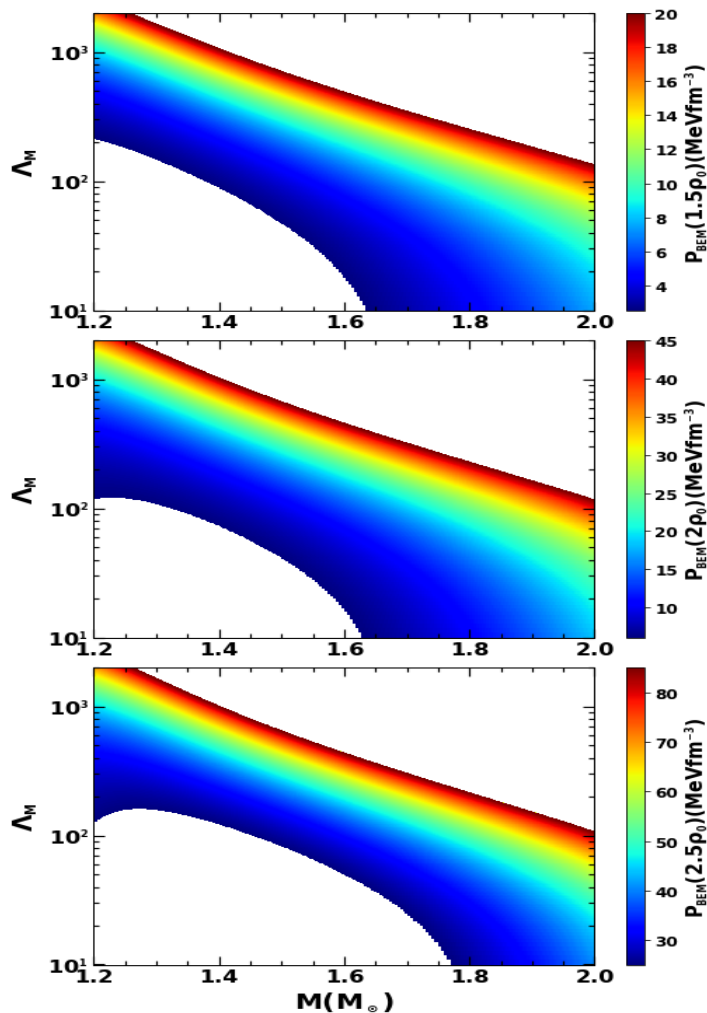


Figure 7. The median values of pressure for β -equilibrated matter at densities $1.5\rho_0$ (top), $2.0\rho_0$ (middle) and $2.5\rho_0$ (bottom) as a function of neutron star mass and tidal deformability.

4. Conclusions

We have used Taylor and $\frac{n}{3}$ expansions of equations of state for symmetric nuclear matter and the β -equilibrated matter to construct marginalized posterior distributions of the nuclear matter parameters which are consistent with the minimal constraints. Only a few low-order nuclear matter parameters, such as the energy per nucleon, incompressibility coefficient for the symmetric nuclear matter and symmetry energy coefficients at the saturation density (ρ_0), are constrained in narrow windows along with the the low density pure neutron matter EoS obtained from a precise next-to-next-to-next-to-leading order (N^3LO) calculation in chiral effective field theory. The tidal deformability, radius and maximum mass are evaluated using large sets minimally constrained EoSs.

The correlations of neutron star properties over a wide range of mass with various key quantities characterising the EoS are investigated. We find that the values of tidal deformability and radius for the neutron star with $1.4M_\odot$ are strongly correlated with the pressure for the β -equilibrated matter and the symmetry energy at density $\sim 2\rho_0$. The radius for $2.07M_\odot$ neutron star is strongly correlated with the pressure for β -equilibrated matter at density $\sim 3\rho_0$. The maximum mass of neutron star is correlated with the pressure for the β -equilibrated matter and symmetric nuclear matter at density $\sim 4.5\rho_0$. This correlation systematics are in harmony with those obtained for unified EoSs for the β -equilibrated matter available for a diverse set of non-relativistic and relativistic mean-field models. We exploit the model independence of correlations to parameterize the pressure for β -equilibrated matter, in the density range 1.5 - $2.5\rho_0$, in terms of the mass and corresponding tidal deformability of neutron star. Such parametric form may facilitate back of the envelope estimation of the pressure at densities around $2\rho_0$ for a given value of tidal deformability of neutron star with mass in the range of 1.2 - $2M_\odot$.

5. Acknowledgements

N.K.P. would like to thank T.K. Jha for constant encouragement and support and gratefully acknowledge the Department of Science and Technology, Ministry of Science and Technology, India, for the support of DST/INSPIRE Fellowship/2019/IF190058. AM acknowledges support from the DST-SERB Start-up Research Grant SRG/2020/001290. The authors sincerely acknowledge the usage of the analysis software BILBY [25,84] and open data from GWOSC [79]. This research has made use of data or software obtained from the Gravitational Wave Open Science Center (gw-openscience.org), a service of LIGO Laboratory, the LIGO Scientific Collaboration, the Virgo Collaboration, and KAGRA. LIGO Laboratory and Advanced LIGO are funded by the United States National Science Foundation (NSF) as well as the Science and Technology Facilities Council (STFC) of the United Kingdom, the Max-Planck-Society (MPS), and the State of Niedersachsen/Germany for support of the construction of Advanced LIGO and construction and operation of the GEO600 detector. Additional support for Advanced LIGO was provided by the Australian Research Council. Virgo is funded, through the European Gravitational Observatory (EGO), by the French Centre National de Recherche Scientifique (CNRS), the Italian Istituto Nazionale di Fisica Nucleare (INFN) and the Dutch Nikhef, with contributions by institutions from Belgium, Germany, Greece, Hungary, Ireland, Japan, Monaco, Poland, Portugal, Spain. The construction and operation of KAGRA are funded by Ministry of Education, Culture, Sports, Science and Technology (MEXT), and Japan Society for the Promotion of Science (JSPS), National Research Foundation (NRF) and Ministry of Science and ICT (MSIT) in Korea, Academia Sinica (AS) and the Ministry of Science and Technology (MoST) in Taiwan.

References

1. Abbott, B. P., *et al.*. Properties of the binary neutron star merger GW170817. *Phys. Rev. X* **2019**, *9*, 011001.
2. Abbott, B. P., *et al.*. Binary Black Hole Population Properties Inferred from the First and Second Observing Runs of Advanced LIGO and Advanced Virgo. *Astrophys. J.* **2019**, *882*, L24.
3. Abbott, B. P., *et al.*. GW190425: Observation of a Compact Binary Coalescence with Total Mass $\sim 3.4 M_{\odot}$. *Astrophys. J.* **2020**, *892*, L3.
4. Abbott, B. P., *et al.*. GW170817: Observation of Gravitational Waves from a Binary Neutron Star Inspiral. *Phys. Rev. Lett.* **2017**, *119*, 161101.
5. Malik, T.; Alam, N.; Fortin, M.; Providência, C.; Agrawal, B.K.; Jha, T.K.; Kumar, B.; Patra, S.K. GW170817: constraining the nuclear matter equation of state from the neutron star tidal deformability. *Phys. Rev. C* **2018**, *98*, 035804.
6. De, S.; Finstad, D.; Lattimer, J.M.; Brown, D.A.; Berger, E.; Biwer, C.M. Tidal Deformabilities and Radii of Neutron Stars from the Observation of GW170817. *Phys. Rev. Lett.* **2018**, *121*, 091102.
7. Fattoyev, F.J.; Piekarewicz, J.; Horowitz, C.J. Neutron Skins and Neutron Stars in the Multimessenger Era. *Phys. Rev. Lett.* **2018**, *120*, 172702.
8. Landry, P.; Essick, R. Nonparametric inference of the neutron star equation of state from gravitational wave observations. *Phys. Rev. D* **2019**, *99*, 084049.
9. Piekarewicz, J.; Fattoyev, F.J. Impact of the neutron star crust on the tidal polarizability. *Phys. Rev. C* **2019**, *99*, 045802.
10. Malik, T.; Agrawal, B.K.; De, J.N.; Samaddar, S.K.; Providência, C.; Mondal, C.; Jha, T.K. Tides in merging neutron stars: Consistency of the GW170817 event with experimental data on finite nuclei. *Phys. Rev. C* **2019**, *99*, 052801.
11. Biswas, B.; Char, P.; Nandi, R.; Bose, S. Towards mitigation of apparent tension between nuclear physics and astrophysical observations by improved modeling of neutron star matter. *Phys. Rev. D* **2020**, *103*, 103015.
12. Thi, H.D.; Mondal, C.; Gulminelli, F. The Nuclear Matter Density Functional under the Nucleonic Hypothesis. *Universe* **2021**, *7*, 373.
13. Watts, A. L., *et al.*. Colloquium: Measuring the neutron star equation of state using x-ray timing. *Rev. Mod. Phys.* **2016**, *88*, 021001.
14. Miller, M. C., *et al.*. PSR J0030+0451 Mass and Radius from NICER Data and Implications for the Properties of Neutron Star Matter. *Astrophys. J.* **2019**, *887*, L24.
15. Riley, T.E., *et al.*. A NICER View of PSR J0030+0451: Millisecond Pulsar Parameter Estimation. *Astrophys. J. Lett.* **2019**, *887*, L21.
16. Zhang, N.B.; Li, B.A.; Xu, J. Combined Constraints on the Equation of State of Dense Neutron-rich Matter from Terrestrial Nuclear Experiments and Observations of Neutron Stars. *Astrophys. J.* **2018**, *859*, 90.
17. Cai, B.J.; Li, B.A. Intrinsic correlations among characteristics of neutron-rich matter imposed by the unbound nature of pure neutron matter. *Phys. Rev. C* **2021**, *103*, 034607.
18. Gil, H.; Papakonstantinou, P.; Hyun, C.H. Constraints on the curvature of nuclear symmetry energy from recent astronomical data within the KIDS framework. *Int. J. Mod. Phys. E* **2022**, *31*, 2250013.
19. Lattimer, J.M.; Prakash, M. Neutron star structure and the equation of state. *Astrophys. J.* **2001**, *550*, 426.
20. Maselli, A.; Cardoso, V.; Ferrari, V.; Gualtieri, L.; Pani, P. Equation-of-state-independent relations in neutron stars. *Phys. Rev. D* **2013**, *88*, 023007.
21. Abbott, B. P., *et al.*. GW170817: Measurements of neutron star radii and equation of state. *Phys. Rev. Lett.* **2018**, *121*, 161101.
22. Lim, Y.; Holt, J.W. Neutron star tidal deformabilities constrained by nuclear theory and experiment. *Phys. Rev. Lett.* **2018**, *121*, 062701.
23. Tsang, C.Y.; Tsang, M.B.; Danielewicz, P.; Lynch, W.G.; Fattoyev, F.J. Insights on Skyrme parameters from GW170817. *Phys. Lett. B* **2019**, *796*, 1.
24. Tsang, C.Y.; Tsang, M.B.; Danielewicz, P.; Lynch, W.G.; Fattoyev, F.J. Impact of the neutron-star deformability on equation of state parameters. *Phys. Rev. C* **2020**, *102*, 045808.
25. Ashton, Gregory, *et al.*. Bilby: A User-friendly Bayesian Inference Library for Gravitational-wave Astronomy. *Astrophys. J. Suppl. Ser.* **2019**, *241*, 27.
26. Biscoveanu, S.; Thrane, E.; Vitale, S. Constraining Short Gamma-Ray Burst Jet Properties with Gravitational Waves and Gamma-Rays. *Astrophys. J.* **2020**, *893*, 38.
27. Coughlin, M.W.; Dietrich, T. Can a black hole-neutron star merger explain GW170817, AT2017gfo, and GRB170817A? *Phys. Rev. D* **2019**, *100*, 043011.
28. Hernandez Vivanco, F.; Smith, R.; Thrane, E.; Lasky, P.D.; Talbot, C.; Raymond, V. Measuring the neutron star equation of state with gravitational waves: The first forty binary neutron star merger observations. *Phys. Rev. D* **2019**, *100*, 103009.
29. Biscoveanu, S.; Vitale, S.; Haster, C.J. The Reliability of the Low-latency Estimation of Binary Neutron Star Chirp Mass. *Astrophys. J.* **2019**, *884*, L32.
30. Lower, M.E.; Thrane, E.; Lasky, P.D.; Smith, R. Measuring eccentricity in binary black hole inspirals with gravitational waves. *Phys. Rev. D* **2018**, *98*, 083028.
31. Romero-Shaw, I.M.; Lasky, P.D.; Thrane, E. Searching for eccentricity: Signatures of dynamical formation in the first gravitational-wave transient catalogue of LIGO and Virgo. *Month. Not. R. Astron. Soc.* **2019**, *490*, 5210.
32. Ramos-Buades, A.; Husa, S.; Pratten, G.; Estellés, H.; García-Quirós, C.; Mateu-Lucena, M.; Colleoni, M.; Jaume, R. First survey of spinning eccentric black hole mergers: Numerical relativity simulations, hybrid waveforms, and parameter estimation. *Phys. Rev. D* **2020**, *101*, 083015.
33. Romero-Shaw, I.M.; Farrow, N.; Stevenson, S.; Thrane, E.; Zhu, X.J. On the origin of GW190425. *Month. Not. R. Astron. Soc.* **2020**, *496*, L64–L69.

34. Zevin, M.; Berry, C.P.L.; Coughlin, S.; Chatziioannou, K.; Vitale, S. You Can't Always Get What You Want: The Impact of Prior Assumptions on Interpreting GW190412. *Astrophys. J.* **2020**, *899*, L17.
35. Keitel, D. Multiple-image Lensing Bayes Factor for a Set of Gravitational-wave Events. *Res. Notes. AAS* **2019**, *3*, 46.
36. Ashton, G.; Khan, S. Multiwaveform inference of gravitational waves. *Phys. Rev. D* **2020**, *101*, 064037.
37. Payne, E.; Talbot, C.; Thrane, E. Higher order gravitational-wave modes with likelihood reweighting. *Phys. Rev. D* **2019**, *100*, 123017.
38. Zhao, Z.C.; Lin, H.N.; Chang, Z. The prospects of using gravitational waves for constraining the anisotropy of the Universe. *Chin. Phys. C* **2019**, *43*, 075102.
39. Wesolowski, S.; Klco, N.; Furnstahl, R.J.; Phillips, D.R.; Thapaliya, A. Bayesian parameter estimation for effective field theories. *J. Phys. G* **2016**, *43*, 074001.
40. Somasundaram, R.; Drischler, C.; Tews, I.; Margueron, J. Constraints on the nuclear symmetry energy from asymmetric-matter calculations with chiral NN and $3N$ interactions. *Phys. Rev. C* **2021**, *103*, 045803.
41. Drischler, C.; Han, S.; Lattimer, J.M.; Prakash, M.; Reddy, S.; Zhao, T. Limiting masses and radii of neutron stars and their implications. *Phys. Rev. C* **2021**, *103*, 045808.
42. Tews, I.; Lattimer, J.M.; Ohnishi, A.; Kolomeitsev, E.E. Symmetry Parameter Constraints from a Lower Bound on Neutron-matter Energy. *Astrophys. J.* **2017**, *848*, 105.
43. Carreau, T.; Gulminelli, F.; Margueron, J. General predictions for the neutron star crustal moment of inertia. *Phys. Rev. C* **2019**, *100*, 055803.
44. Thi, H.D.; Carreau, T.; Fantina, A.F.; Gulminelli, F. Uncertainties in the pasta-phase properties of catalysed neutron stars. *Astron. Astrophys.* **2021**, *654*, A114.
45. Riley, T.E.; Raaijmakers, G.; Watts, A.L. On parametrized cold dense matter equation-of-state inference. *Month. Not. R. Astron. Soc.* **2018**, *478*, 1093.
46. Raaijmakers, G.; Others. Constraining the dense matter equation of state with joint analysis of NICER and LIGO/Virgo measurements. *Astrophys. J. Lett.* **2020**, *893*, L21.
47. Jiang, J.L.; Tang, S.P.; Wang, Y.Z.; Fan, Y.Z.; Wei, D.M. PSR J0030+0451, GW170817 and the nuclear data: joint constraints on equation of state and bulk properties of neutron stars. *Astrophys. J.* **2020**, *892*, 1.
48. Güven, H.; Bozkurt, K.; Khan, E.; Margueron, J. Multimessenger and multiphysics Bayesian inference for the GW170817 binary neutron star merger. *Phys. Rev. C* **2020**, *102*, 015805.
49. Biswas, B. Impact of PREX-II and Combined Radio/NICER/XMM-Newton's Mass-radius Measurement of PSR J0740+6620 on the Dense-matter Equation of State. *Astrophys. J.* **2021**, *921*, 63.
50. Landry, P.; Essick, R.; Chatziioannou, K. Nonparametric constraints on neutron star matter with existing and upcoming gravitational wave and pulsar observations. *Phys. Rev. D* **2020**, *101*, 123007.
51. Huth, S., et al. Constraining Neutron-Star Matter with Microscopic and Macroscopic Collisions **2021**. [[arXiv:nucl-th/2107.06229](https://arxiv.org/abs/2107.06229)].
52. Biswas, B. Bayesian Model Selection of Neutron Star Equations of State Using Multi-messenger Observations. *Astrophys. J.* **2022**, *926*, 75.
53. Imam, S.M.A.; Patra, N.K.; Mondal, C.; Malik, T.; Agrawal, B.K. Bayesian reconstruction of nuclear matter parameters from the equation of state of neutron star matter. *Phys. Rev. C* **2022**, *105*, 015806.
54. Chen, L.W.; Ko, C.M.; Li, B.A. Nuclear matter symmetry energy and the neutron skin thickness of heavy nuclei. *Phys. Rev. C* **2005**, *72*, 064309.
55. Chen, L.W.; Cai, B.J.; Ko, C.M.; Li, B.A.; Shen, C.; Xu, J. High-order effects on the incompressibility of isospin asymmetric nuclear matter. *Phys. Rev. C* **2009**, *80*, 014322.
56. Newton, W.G.; Hooker, J.; Gearheart, M.; Murphy, K.; Wen, D.H.; Fattoyev, F.J.; Li, B.A. Constraints on the symmetry energy from observational probes of the neutron star crust. *Eur. Phys. J. A* **2014**, *50*, 41.
57. Margueron, J.; Hoffmann Casali, R.; Gulminelli, F. Equation of state for dense nucleonic matter from metamodeling. I. Foundational aspects. *Phys. Rev. C* **2018**, *97*, 025805.
58. Margueron, J.; Gulminelli, F. Effect of high-order empirical parameters on the nuclear equation of state. *Phys. Rev. C* **2019**, *99*, 025806.
59. Lattimer, J.M.; Prakash, M. The Equation of State of Hot, Dense Matter and Neutron Stars. *Phys. Rept.* **2016**, *621*, 127.
60. Gil, H.; Papakonstantinou, P.; Hyun, C.H.; Park, T.S.; Oh, Y. Nuclear Energy Density Functional for KIDS. *Acta Phys. Polon. B* **2017**, *48*, 305.
61. Gelman, A.; Carlin, J.B.; Stern, H.S.; Dunson, D.B.; Vehtari, A.; Rubin, D.B.; Carlin, J.; Stern, H.; Rubin, D.; Dunson, D. *Bayesian Data Analysis Third edition*; CRC Press, Boca Raton, Florida, 2013.
62. Buchner, J.; Georgakakis, A.; Nandra, K.; Hsu, L.; Rangel, C.; Brightman, M.; Merloni, A.; Salvato, M.; Donley, J.; Kocevski, D. X-ray spectral modelling of the AGN obscuring region in the CDFS: Bayesian model selection and catalogue. *Astron. Astrophys.* **2014**, *564*, 015805.
63. Chabanat, E.; Bonche, P.; Haensel, P.; Meyer, J.; Schaeffer, R. A Skyrme parametrization from subnuclear to neutron star densities. 2. Nuclei far from stabilities. *Nucl. Phys. A* **1998**, *635*, 231.
64. Chabanat, E.; Bonche, P.; Haensel, P.; Meyer, J.; Schaeffer, R. A Skyrme parametrization from subnuclear to neutron star densities. *Nucl. Phys. A* **1997**, *627*, 710.
65. Hebeler, K.; Lattimer, J.M.; Pethick, C.J.; Schwenk, A. Equation of state and neutron star properties constrained by nuclear physics and observation. *Astrophys. J.* **2013**, *773*, 11.

-
66. Reed, B.T.; Fattoyev, F.J.; Horowitz, C.J.; Piekarewicz, J. Implications of PREX-2 on the Equation of State of Neutron-Rich Matter. *Phys. Rev. Lett.* **2021**, *126*, 172503.
 67. Adhikari, D., *et al.*. Accurate Determination of the Neutron Skin Thickness of ^{208}Pb through Parity-Violation in Electron Scattering. *Phys. Rev. Lett.* **2021**, *126*, 172502.
 68. Oppenheimer, J.R.; Volkoff, G.M. On massive neutron cores. *Phys. Rev.* **1939**, *55*, 374.
 69. Tolman, R.C. Static solutions of Einstein's field equations for spheres of fluid. *Phys. Rev.* **1939**, *55*, 364.
 70. Baym, G.; Pethick, C.; Sutherland, P. The Ground state of matter at high densities: Equation of state and stellar models. *Astrophys. J.* **1971**, *170*, 299.
 71. Carriere, J.; Horowitz, C.J.; Piekarewicz, J. Low mass neutron stars and the equation of state of dense matter. *Astrophys. J.* **2003**, *593*, 463–471.
 72. Fortin, M.; Providencia, C.; Raduta, A.R.; Gulminelli, F.; Zdunik, J.L.; Haensel, P.; Bejger, M. Neutron star radii and crusts: uncertainties and unified equations of state. *Phys. Rev. C* **2016**, *94*, 035804.
 73. Piekarewicz, J.; Fattoyev, F.J. Impact of the neutron star crust on the tidal polarizability. *Phys. Rev. C* **2019**, *99*, 045802.
 74. Miller, M. C., *et al.*. The Radius of PSR J0740+6620 from NICER and XMM-Newton Data. *Astrophys. J. Lett.* **2021**, *918*, L28.
 75. Riley, Thomas E., *et al.*. A NICER View of the Massive Pulsar PSR J0740+6620 Informed by Radio Timing and XMM-Newton Spectroscopy. *Astrophys. J. Lett.* **2021**, *918*, L27.
 76. Romani, R.W.; Kandel, D.; Filippenko, A.V.; Brink, T.G.; Zheng, W. PSR J1810+1744: Companion Darkening and a Precise High Neutron Star Mass. *Astrophys. J. Lett.* **2021**, *908*, L46.
 77. Abbott, B. P., *et al.*. GW170817: Measurements of Neutron Star Radii and Equation of State. *Phys. Rev. Lett.* **2018**, *121*, 161101.
 78. Abbott, B. P., *et al.*. Properties of the binary neutron star merger GW170817. *Phys. Rev. X* **2019**, *9*, 011001.
 79. Abbott, R., *et al.*; LIGO Scientific Collaboration. Open data from the first and second observing runs of Advanced LIGO and Advanced Virgo. *SoftwareX* **2021**, *13*, 100658.
 80. Riley, Thomas E., *et al.*. A NICER View of PSR J0030+0451: Millisecond Pulsar Parameter Estimation. *Astrophys. J. Lett.* **2019**, *887*, L21.
 81. Miller, M. C., *et al.*. PSR J0030+0451 Mass and Radius from NICER Data and Implications for the Properties of Neutron Star Matter. *Astrophys. J. Lett.* **2019**, *887*, L24.
 82. Malik, T.; Ferreira, M.; Agrawal, B.K.; Providência, C. Relativistic description of dense matter equation of state and compatibility with neutron star observables: a Bayesian approach **2022**. [[arXiv:nucl-th/2201.12552](https://arxiv.org/abs/2201.12552)].
 83. Ferreira, M.; Fortin, M.; Malik, T.; Agrawal, B.K.; Providência, C. Empirical constraints on the high-density equation of state from multimessenger observables. *Phys. Rev. D* **2020**, *101*, 043021.
 84. Romero-Shaw, I. M., *et al.*. Bayesian inference for compact binary coalescences with BILBY- validation and application to the first LIGO-Virgo gravitational-wave transient catalogue. *Mon. Not. Roy. Astron. Soc.* **2020**, *499*, 3295.